Rational Design of Near-Infrared Carbon Dots as Polarity-Sensitive Fluorescent Probe and Imaging of Lipid Droplet

Zheng Yang[a,b,*], Ying Peng[a], Mengyao Qu[a], Haonan Yang[a], Xiaodan Jia[a,b], and Xiangrong Liu[a,b]

[a] *College of Chemistry and Chemical Engineering, Xi'an University of Science and Technology, Xi'an 710054, P. R. China.*

[b] *Key Laboratory of Coal Resources Exploration and Comprehensive Utilization, Ministry of Land and Resources, Xi'an 710012, P. R. China.*

*Corresponding author: yangzheng@xust.edu.cn; orcid.org/0000-0002-1554-4794

CONTENTS

1. Experimental Section

1.1. General methods

The fluorescent spectra were performed on the Horiba FluoroMax–4 fluorescence spectrophotometer. Absorbance spectra were recorded on the Hitachi U–2900 spectrophotometer. Fluorescent decays were obtained on an Edinburgh FLSP920 steady/transient fluorescence spectrometer. Transmission electron microscope images were performed from a JEM–1400 Flash analyzer. Raman spectra were measured with ThermoFisher DXR 2 spectroscopy. X–ray photoelectron spectroscopy spectra were conducted on a ULVAC–PHI PHI5000VersaProbeIII spectrophotometer with the excitation source of Al Ka. X–Ray powder diffraction spectroscopy analyses were recorded on the Bruker D8 Advance analyzer. IR spectra were performed on a Bruker Tensor 27 spectrometer. NMR spectra were recorded on a Varian Inova–400 MHz spectrometer (at 400 MHz for 1H) with tetramethylsilane (TMS) as internal standard. Bioimaging of the sensors were conducted on an Olympus FV1000 confocal microscopn and the excitation wavelength was set as 408 nm. The cell viability was determined at 405 nm absorbance using an ELx800 Absorbance Reader (BioTek Instruments, Inc.). Xe lamp irradiation was performed by the CEL–HXF300–T3 Xenon lamp source system with the light intensity of 1500 mW/cm^2.

2,7-dihydroxynaphthalene, benzoic acid and selenomethionine (Se-Met) were obtained from *Inno–Chem Co., LTD.* (Beijing, China). All other reagents, including various metallic compounds were purchased from *Daosheng Biochemical Science and Trade Co., LTD* (Xi'an, China). Organic reagents and solutions were purchased from

Zhiyuan and *Tianli Co., LTD* (Tianjin, China). All chemicals are of analytical grade and used without further purification.

1.2. Synthesis of the CDs

0.5 g of benzoic acid, 0.4 g of 2,7-dihydroxynaphthalene and 0.6 g of Se-Met were added into a mixture solution of 10 mL of dimethylformamide (DMF) and 10 mL of deionized water. The mixture was then sonicated for 10 min until completely dissolved and was put into a 50 mL polyethylene Teflon-lined autoclave and heated at 180 ℃ for 6 h. After cooling to room temperature, the solution was centrifuged at 10000 rpm for 5 min, and the supernatant was filtered through a 0.2 mm microporous filter membrane to obtain the filtrate. The filtrate was then washed for several times with saturated salt solution and dialyzed against ultrapure water (1000 Da, molecular weight cutoff) for 24 h to remove unreacted micromolecule reagents. The final product was freeze–dried under vacuum to obtain a solid sample, which is stored in a refrigerator at 0 ℃ for future use.

1.3 Fluorescence detection of polarity

1.3.1 Polarity sensitivity in different solutions

Stock solution of the CDs was prepared in DMF at the concentration of 100 $mg \cdot L^{-1}$. To inspect the polarity selectivity, 0.10 mL of the stock solution was added to the 10.00 mL volumetric flask and then diluted to the mark with different reagents including: cyclohexane (CYH), 1,4-dioxolane (DOX), ethyl acetate (EA), tetrahydrofuran (THF), dichloromethane (DCM), dimethylsulfoxide (DMSO), acetone (AC), , ethanol (EtOH), methanol (MeOH), DMF and H_2O. The absorbance and

fluorescent spectra were then recorded.

1.3.2 Polarity sensitivity in different ratios of DOX-H_2O solutions

Stock solution of the CDs was prepared in DMF at the concentration of 100 mg·L^{-1}. To inspect the polarity selectivity, 0.10 mL of the stock solution was added to the 10.00 mL volumetric flask and then diluted to the mark with different ratios of DOX-H_2O solutions in which the containing of H_2O varies from 0% to 99%. The absorbance and fluorescent spectra were then recorded.

1.4 Biological imaging in living cells

1.4.1 Cytotoxicity testing of the CDs.

HeLa cells were cultured in 96-well plates for 24 h at 37 ℃ in 5% CO_2 (the medium was Dulbecco's modified Eagle's medium (DMEM) containing 1% penicillin/ streptomycin and 10% fetal bovine serum). The old DMEM was then removed and fresh DMEM with 100 mL of different concentrations of CDs solution (0–100 mg·mL^{-1}) was added to the cells and incubated for 24 h under the same conditions. Then 10 mL of 3-(4,5)-dimethylthiahiazo(-z-y1)-3,5-di-phenytetrazoliumromide (MTT) solution was added to each well and the incubation was continued for 4 h. Finally, the absorbance of each well was recorded using a microtiter reader to assess the cytotoxicity of the CDs.

1.4.2 Time dependent testing of the CDs.

The CDs (50 μg·mL^{-1}) was incubated with the HeLa cells for different incubation times as 0 min, 1 min, 3 min, 5 min, 10 min, 15 min, and 30 min. The changes of the fluorescence intensity were recorded by confocal laser scanning microscope (CLSM)

to observe the change of fluorescence intensity to the maximum value.

1.4.3 Concentration dependent testing of the CDs.

Confocal images were taken at different concentration of CDs (0 μg·mL^{-1}, 10 μg·mL^{-1}, 20 μg·mL^{-1}, 30 μg·mL^{-1}, 40 μg·mL^{-1}, 50 μg·mL^{-1}, and 60 μg·mL^{-1}) incubating with the HeLa cells for 10 min to observe the range of fluorescence maximum values. The changes of the fluorescence intensity were recorded by CLSM.

1.4.4 Subcellular organelle co-localization of the CDs.

As in the process of culturing cells above, the cultured HeLa cells were incubated with the CDs in DMEM for 10 min at 37 ℃, 5% CO_2, and then treated with commercial dyes Lyso-Tracker Green (100 nmol·mL^{-1}, targeting lysosomes), Mito-Tracker Green FM (100 nmol·mL^{-1}, targeting mitochondria) and Bodipy493/503 (100 nmol·mL^{-1}, targeting lipid droplet) for 10 min. Cells were then washed 3 times with phosphate-buffered (PBS) and 1 mL of serum-free DMEM was added. Cells were finally subjected to the CLSM.

1.4.5 Study on the cellular energy dependence mechanism of the CDs.

The HeLa cells were pretreated at low temperature for 4 hours, and then incubated with 50 μg·mL^{-1} of CDs to observe the fluorescence intensity. In another group, the cells were pretreated at low temperature for 4 h, and then incubated with 50 μg·mL^{-1} of CDs and NaN_3 to observe the fluorescence intensity by CLSM.

1.4.6 Study on the endocytosis mechanism of the CDs.

HeLa cells were pretreated with 100 μg·mL^{-1} Chlorpromazine (CPZ), 10 μg·mL^{-1} Methyl-β-cyclodextrin (MβCD), 20 μg·mL^{-1} amiloride (AMI) and 100 μg·mL^{-1}

genistine (Gen) for 4 hours, and then incubated with the CDs (30 μg·mL^{-1}) for another 4h. Then the fluorescence intensity of the four groups of cells were observed and recorded by CLSM.

1.4.7 Detection of cell polarity by the CDs.

As in the process of culturing cells above, cultured HeLa cells were stained with 50 mg·mL^{-1} CDs solution were used as the control group. Then the HeLa cells stained by 50 mg·mL^{-1} CDs solution with the addition of 5 mmol·L^{-1} dithiothreitol (DTT) were used as the experimental group, and the change in cell polarity was detected by observing the intensity of fluorescence intensity in 0 min, 1 min, 3 min, 5 min, 10 min, 25 min, and 30 min by CLSM.

1.4.8 Biological imaging in zebrafish by the CDs.

Fluorescent imaging in living zebrafish were performed in the similar procedures. The zebrafish were cultured in DMEM supplemented with 10% FBS, at 37 ℃ in the humidified atmosphere with 5% CO_2 and 95% air for 4 h. The growth medium was then removed and the zebrafish were washed with DMEM without FBS and imaged. The zebrafish were then incubated with 50 mg·mL^{-1} of the CDs for 10 min at 37 ℃, washed three times with PBS and imaged by CLSM.

2. Optical properties of the probe.

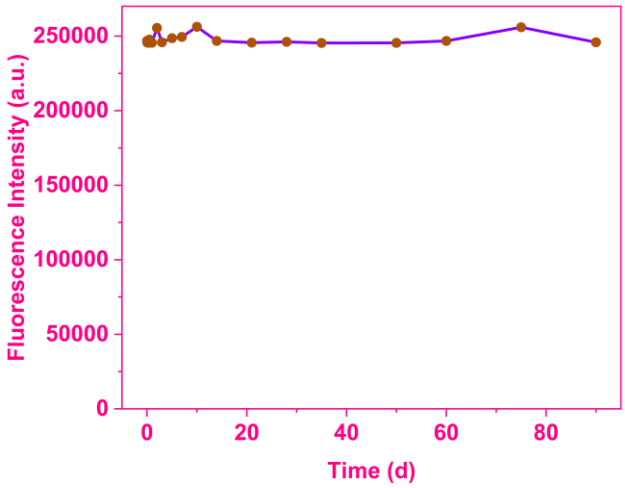

Fig. S1. Fluorescent intensity of CDs at different storage times. λ_{ex} = 550 nm.

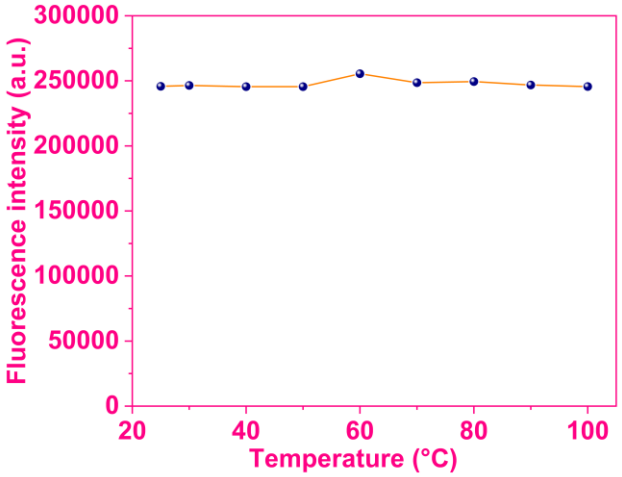

Fig. S2. The fluorescence stability of the CDs in high temperature. λ_{ex} = 550 nm.

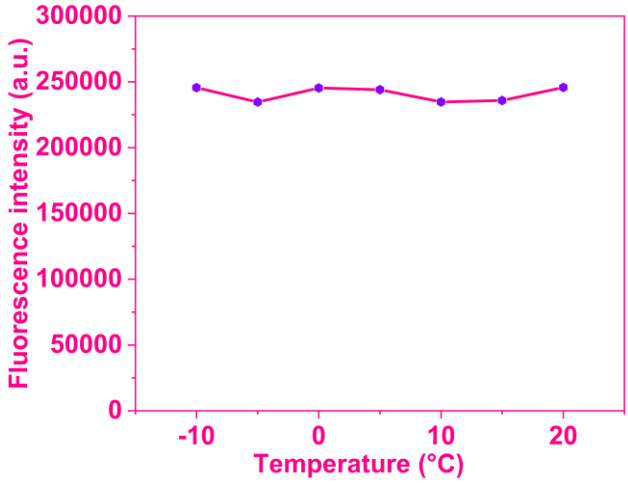

Fig. S3. The fluorescence stability of the CDs in low temperature. λ_{ex} = 550 nm.

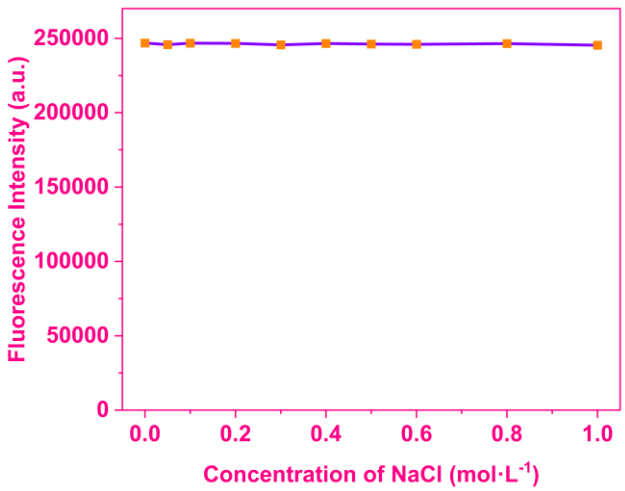

Fig. S4. Fluorescent intensity of CDs at different concentrations of NaCl. λ_{ex} = 550 nm.

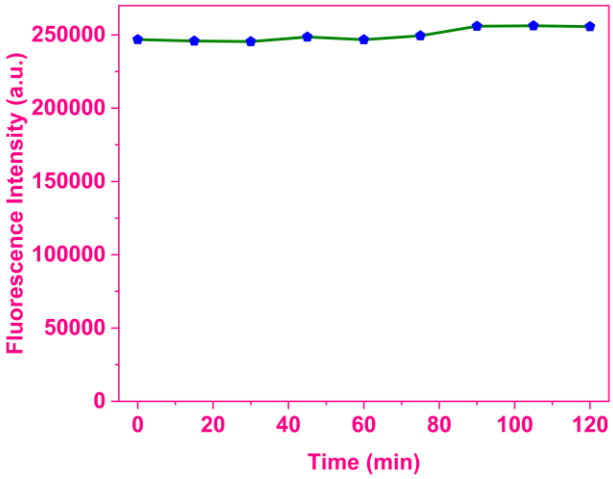

Fig. S5. Fluorescent intensity of CDs at different irradiation time under Xe lamp. λ_{ex} = 550 nm.

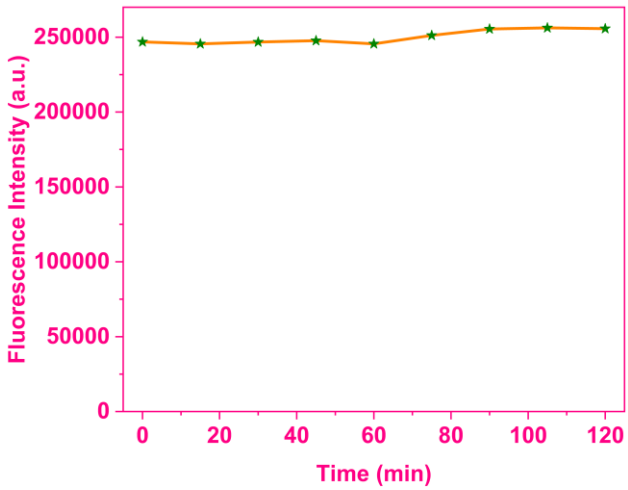

Fig. S6. Fluorescent intensity of CDs at different irradiation time under UV lamp. λ_{ex} = 550 nm.

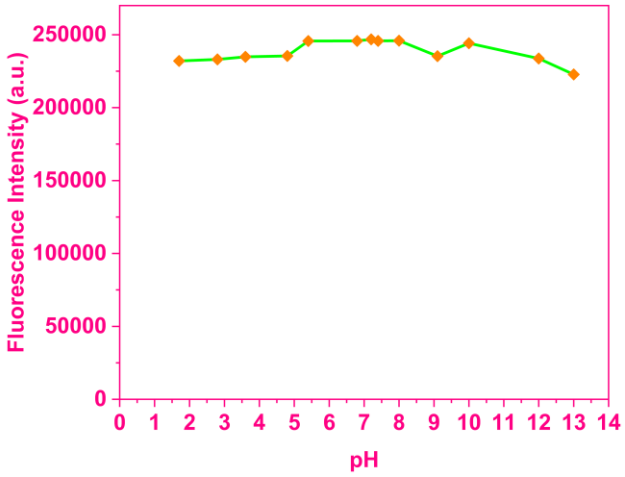

Fig. S7. Fluorescent intensity of the CDs in different pH value. λ_{ex} = 550 nm.

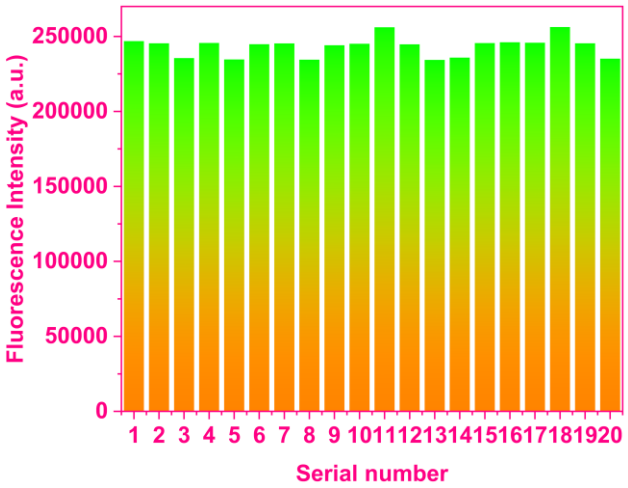

Fig. S8. The fluorescence stability of the CDs in cations. 1, blank, 2, Li^+, 3, Na^+, 4, K^+, 5, Ag^+, 6, Ca^{2+}, 7, Mg^{2+}, 8, Cu^{2+}, 9, Cd^{2+}, 10, Mn^{2+}, 11, Fe^{2+}, 12, Co^{2+}, 13, Ni^{2+}, 14, Zn^{2+}, 15, Pb^{2+}, 16, Hg^{2+}, 17, Fe^{3+}, 18, Cr^{3+}, 19, Al^{3+}, 20, Sn^{4+}. 20, $O_2^{\cdot-}$, 21, H_2O_2, 22, NO, 23, $ONOO^-$, 24, NO_3^-, 25, PO_4^{3-}, 26, CO_3^{2-}, 27, OAc^-, 28, $C_2O_4^{2-}$, 29, ClO^-, 30, GSH. λ_{ex} = 550 nm.

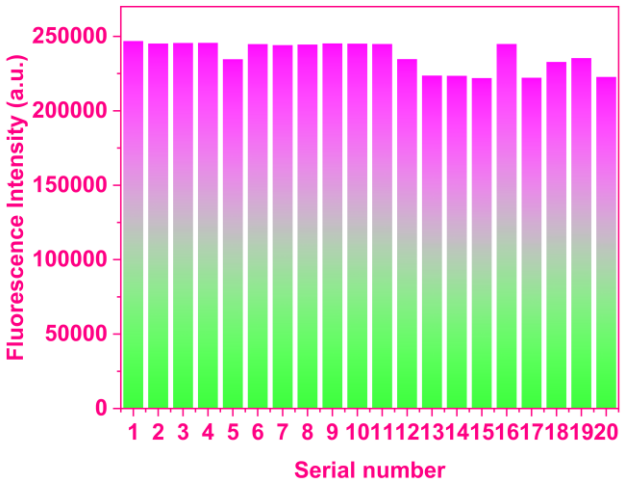

Fig. S9. The fluorescence stability of the CDs in anions and active molecules. 1, blank, 2, AMP, 3, ADP, 4, ATP, 5, Cys, 6, GSH, 7, Hcy, 8, $O_2^{\cdot-}$, 9, H_2O_2, 10, NO, 11, H_2S, 12, $ONOO^-$, 13, ClO^-, 14, PO_4^{3-}, 15, CO_3^{2-}, 16, OAc^-, 17, $C_2O_4^{2-}$, 18, SO_3^{2-}, 19, dopamine, 20, ascorbic acid. λ_{ex} = 550 nm.

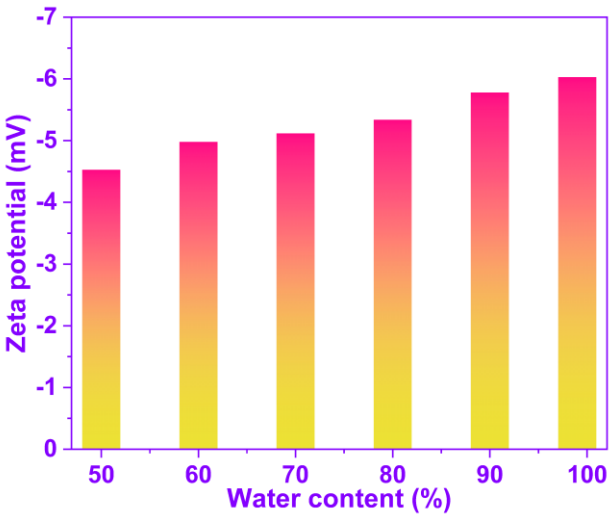

Fig. S10. The Zeta potentials of the CDs in different ratios 1,4-dioxane/H_2O mixed solvents.

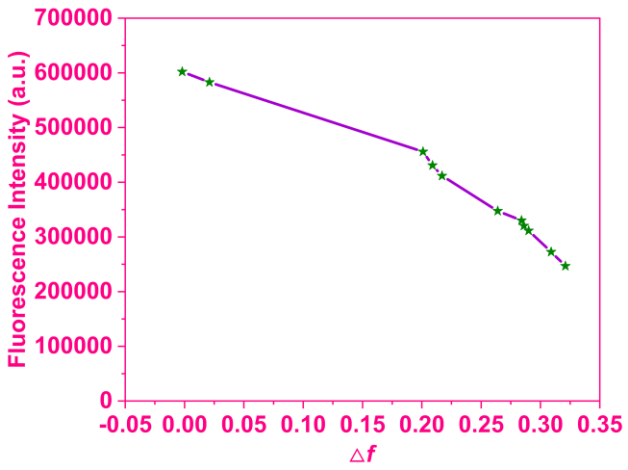

Fig. S11. Fluorescence intensity of the CDs in the solvents with different polarity. λ_{ex} = 550 nm.

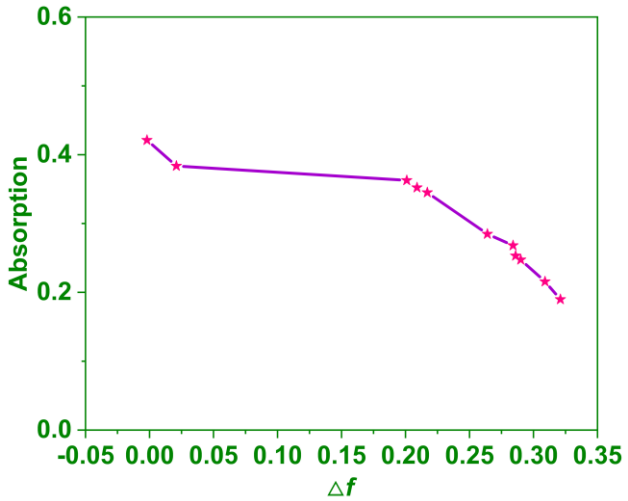

Fig. S12. Absorption intensity of the CDs in the solvents with different polarity.

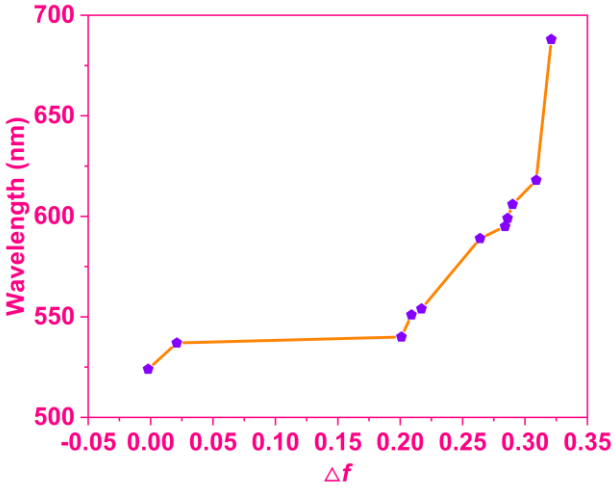

Fig. S13. Fluorescence wavelengths of the CDs in the solvents with different polarity. λ_{ex} = 550 nm.

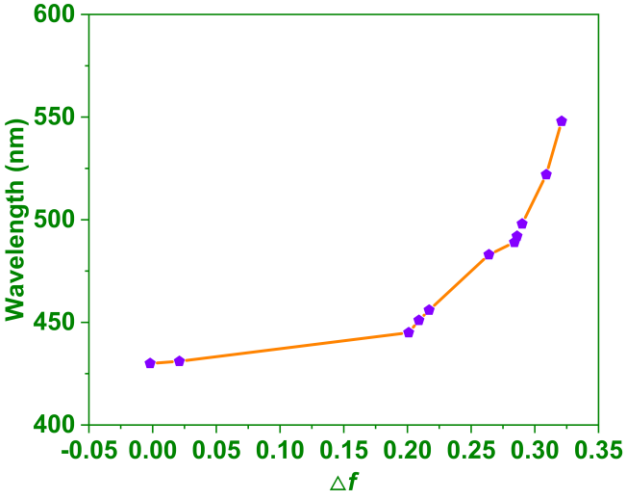

Fig. S14. Absorption wavelengths of the CDs in the solvents with different polarity.

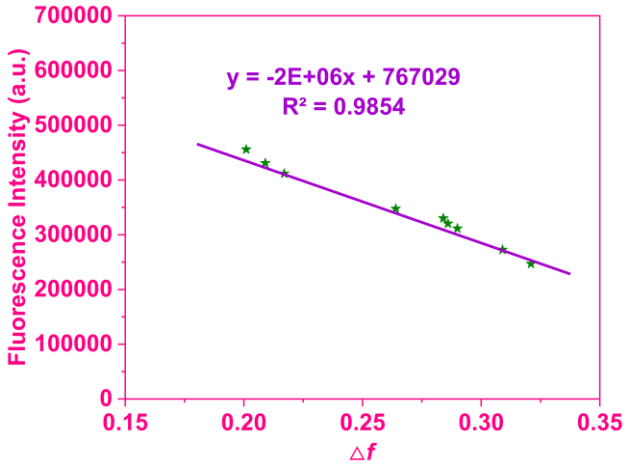

Fig. S15. Linear relationship between fluorescence intensity of the CDs and the solvents with different polarity. λ_{ex} = 550 nm.

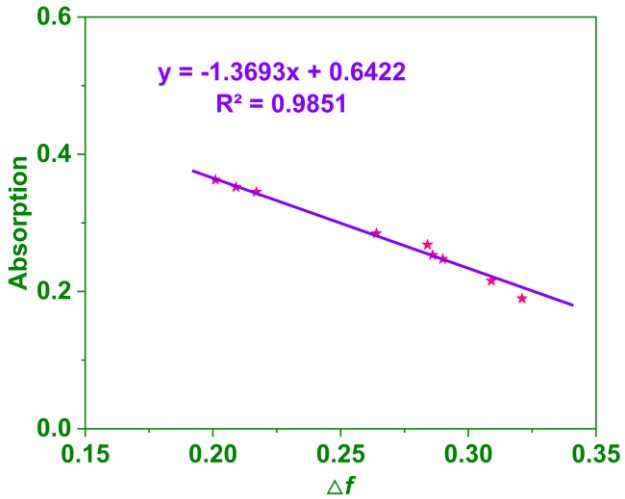

Fig. S16. Linear relationship between absorption intensity of the CDs and the solvents with different polarity.

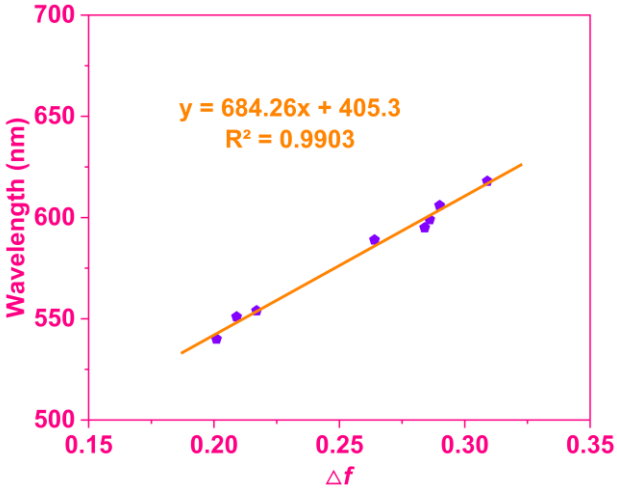

Fig. S17. Linear relationship between fluorescence wavelengths of the CDs and the solvents with different polarity. λ_{ex} = 550 nm.

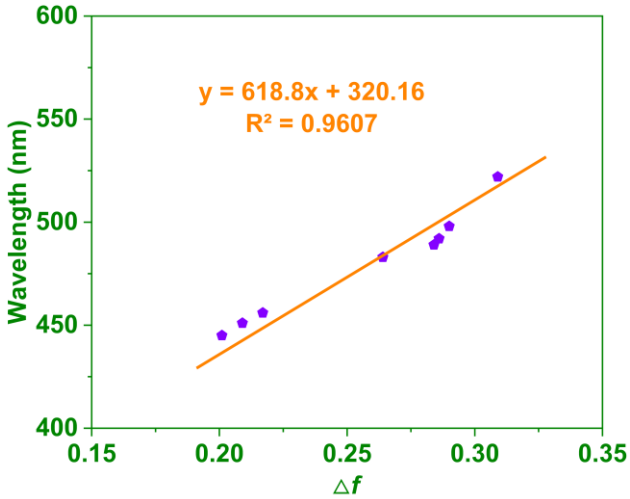

Fig. S18. Linear relationship between absorption wavelengths of the CDs and the solvents with different polarity.

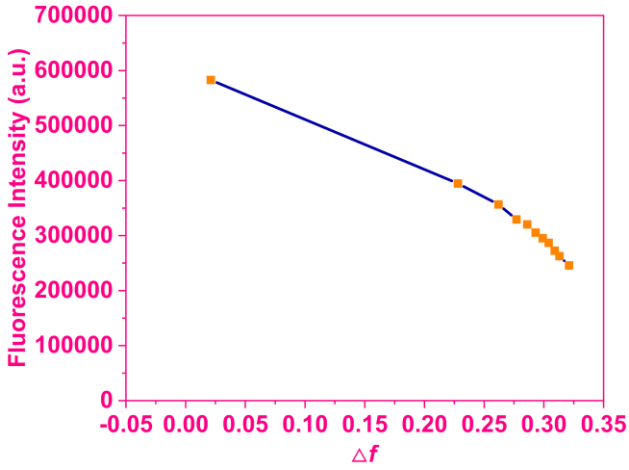

Fig. S19. Fluorescence intensity of the CDs and in different ratios 1,4-dioxane/H_2O mixed solvents. λ_{ex} = 550 nm.

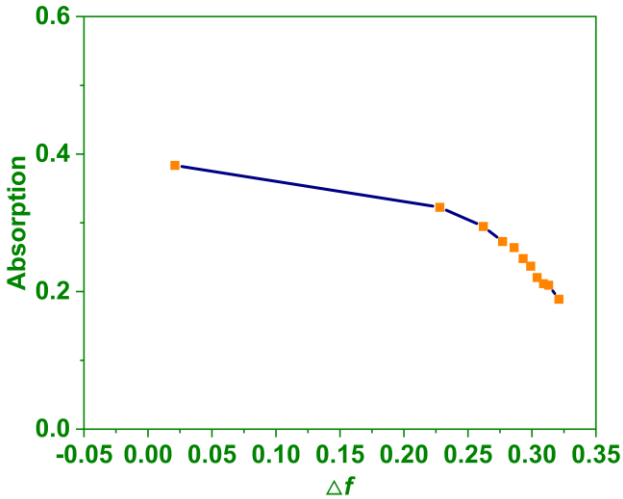

Fig. S20. Absorption intensity of the CDs in different ratios 1,4-dioxane/H_2O mixed solvents.

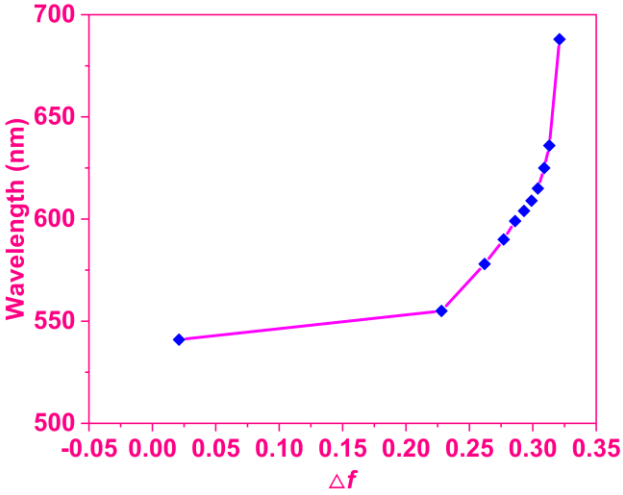

Fig. S21. Fluorescence wavelengths of the CDs and in different ratios 1,4-dioxane/H_2O mixed solvents. λ_{ex} = 550 nm.

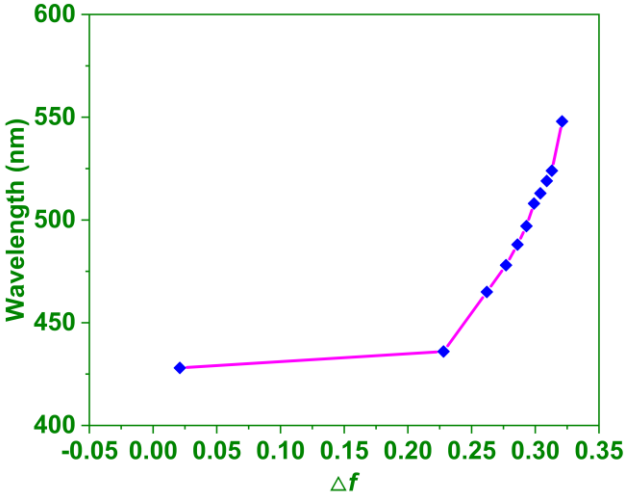

Fig. S22. Absorption wavelengths of the CDs in different ratios 1,4-dioxane/H_2O mixed solvents.

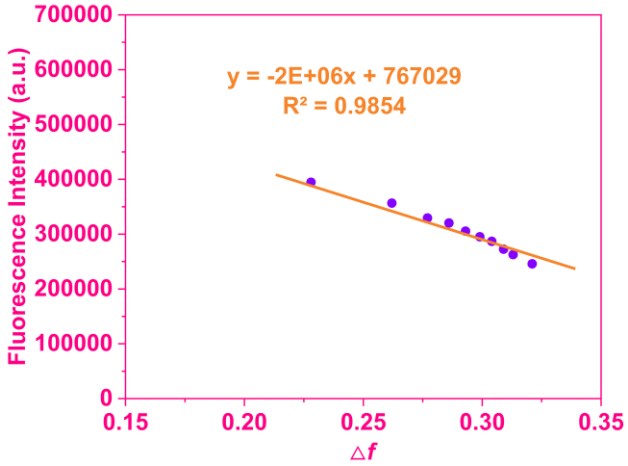

Fig. S23. Linear relationship between fluorescence intensity of the CDs and the polarity of different ratios 1,4-dioxane/H_2O mixed solvents. λ_{ex} = 550 nm.

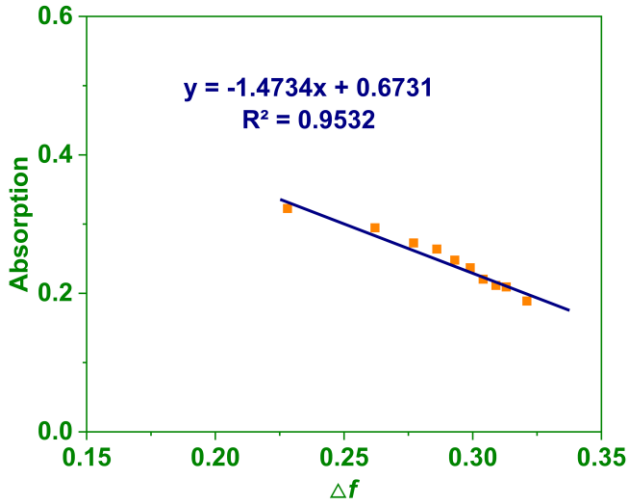

Fig. S24. Linear relationship between absorption intensity of the CDs and the polarity of different ratios 1,4-dioxane/H_2O mixed solvents.

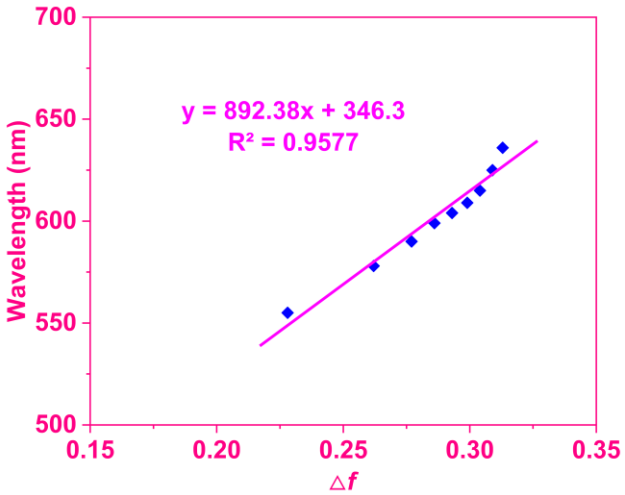

Fig. S25. Linear relationship between fluorescence wavelengths of the CDs and the polarity of different ratios 1,4-dioxane/H_2O mixed solvents. λ_{ex} = 550 nm.

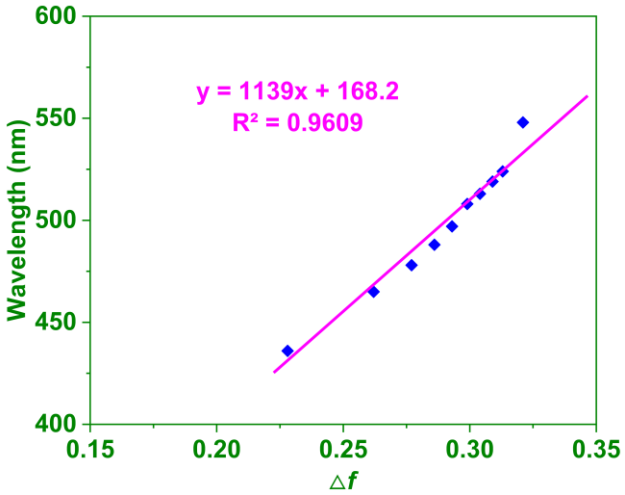

Fig. S26. Linear relationship between absorption wavelengths of the CDs and the polarity of different ratios 1,4-dioxane/H_2O mixed solvents.

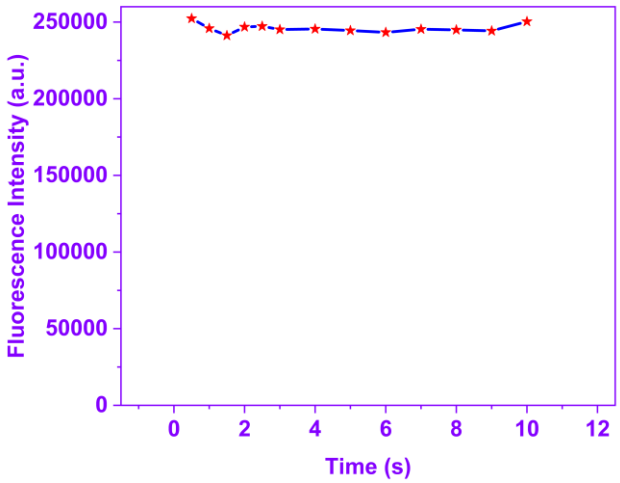

Fig. S27. Response time of fluorescence intensity of CDs to polarity.

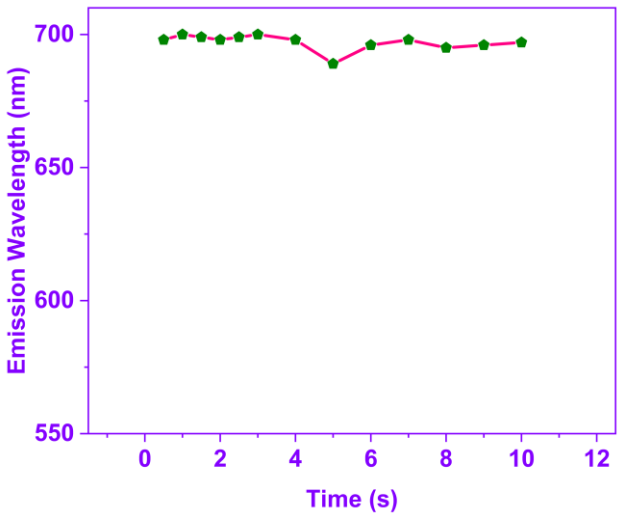

Fig. S28. Response time of emission wavelength of CDs to polarity.

3 Equations about fluorescence lifetime, quantum yield, and polarity.

3.1 Equations for calculation of fluorescence lifetime

$$\tau=\tau_1 B_1 + \tau_2 B_2$$

B_1, B_2 stand for fractional intensities; τ_1, τ_2 are decay times.

3.2 Equations for calculation of quantum yield

$$\varphi_s = \varphi_R \frac{F_S\, A_R}{F_R\, A_S} \frac{\eta_S^2}{\eta_R^2}$$

φ stands for the fluorescence quantum yield, F refers to the integrated fluorescence intensity, and A is the absorption values. The subscript "R" and "S" correspond to the reference and the sample.

3.3 Equations for calculation of polarity

For the polarity of different solvents:

$$\Delta f = \frac{\varepsilon - 1}{2\varepsilon + 1} - \frac{n^2 - 1}{2n^2 + 1}$$

ε is represent dielectric constant, n refers refractive index, Δf means polarity.

For the polarity of the different ratios 1,4-dioxane/H_2O mixed solvents:

$$\varepsilon_{mix} = f_a \varepsilon_a + f_b \varepsilon_b$$

$$n_{mix} = f_a n_a^2 + f_b n_b^2$$

$$\Delta f = \frac{\varepsilon_{mix} - 1}{2\varepsilon_{mix} + 1} - \frac{n_{mix}^2 - 1}{2n_{mix}^2 + 1}$$

ε is represent dielectric constant, n refers refractive index, Δf means polarity.

Table S1. Calculated polarity of the solvents and detected absorption and emission wavelengths of the CDs in related solvents.

Sample	Solvent	ε	n^2	Δf [a]	Abs (nm)	Em (nm)
1	Cyclohexane	2.020	2.034	-0.002	430	524
2	1,4-Dioxane	2.219	2.023	0.021	431	537
3	Ethyl Acetate	6.081	1.882	0.201	445	540
4	Tetrahydrofuran	2.510	1.980	0.209	451	551
5	Dichloromethane	8.930	2.029	0.217	456	554
6	Dimethylsulfoxide	47.240	2.184	0.264	483	589
7	Acetone	20.700	1.846	0.284	489	595
8	Dimethyl Formamide	37.780	1.952	0.286	492	599
9	Ethanol	25.320	1.853	0.290	498	606
10	Methanol	33.000	1.766	0.309	522	618
11	Water	80.400	1.777	0.321	548	688

a $$\Delta f = \frac{\varepsilon - 1}{2\varepsilon + 1} - \frac{n^2 - 1}{2n^2 + 1}$$

ε is represent dielectric constant, n refers refractive index, Δf means polarity.

Table S2. Calculated polarity of different ratios 1,4-dioxane/H_2O mixed solvents and detected absorption and emission wavelengths of the CDs in related solvents.

Sample	1,4-dioxane	H_2O	ε_{mix} [a]	n^2_{mix} [b]	Δf [c]	Abs (nm)	Em (nm)
1	100%	0%	2.219	2.023	0.021	428	541
2	90%	10%	9.825	1.994	0.228	436	555
3	80%	20%	17.444	1.972	0.262	465	578
4	70%	30%	25.055	1.950	0.277	478	590
5	60%	40%	32.670	1.928	0.286	488	599
6	50%	50%	40.285	1.906	0.293	497	604
7	40%	60%	47.900	1.884	0.299	508	609
8	30%	70%	55.515	1.862	0.304	513	615
9	20%	80%	63.130	1.839	0.309	519	625
10	10%	90%	70.745	1.818	0.313	524	636
11	1	99%	80.400	1.777	0.321	548	688

a $\varepsilon_{mix} = f_a\varepsilon_a + f_b\varepsilon_b$

b $n_{mix} = f_a n_a^2 + f_b n_b^2$

c $$\Delta f = \frac{\varepsilon_{mix} - 1}{2\varepsilon_{mix} + 1} - \frac{n_{mix}^2 - 1}{2n_{mix}^2 + 1}$$

ε is represent dielectric constant, n refers refractive index, Δf means polarity.

4. Calculation details.

The calculations of all the structures were performed with B3LYP function via Gaussian 09 Program. The structures were optimized with a combination of basis of double-ζ quality consisting of 6-31G* for C, H elements, 6-31G** for N, Se, O elements. The complex the CDs with Fe^{3+} (S_0 and S_1 state) was optimized with a combination of basis of double-ζ quality consisting of 6-31G* for C, H elements, 6-3G** for N, Se, O elements. All the optimized structures were confirmed to be local minimums due to the non-existence of imaginary frequency. Frequency analysis was not performed for excited state on account of the exhausting mumerical calculation of the force constant for such a large system. The environmental effect of the complex was via PCM model with the solvent molecule.

Table S3. The HOMO and LUMO energy and calculated absorption and emission wavelength of the supposed structures of the CDs.

	HOMO (eV)	LUMO (eV)	△ (eV)	Abs (nm)	Opt (nm)
1	-5.34377	-2.69338	-2.65039	387.23	571.51
2	-5.19139	-2.56359	-2.62780	389.32	575.53
3	-5.45970	-2.39624	-3.06346	335.44	517.17
4	-5.35412	-2.51216	-2.84196	367.75	534.32
5	-4.96009	-2.83380	-2.12630	432.84	727.41
6	-4.87220	-2.73719	-2.13501	421.73	690.84
7	-5.25643	-2.65638	-2.60005	386.21	590.13
8	-4.73506	-2.83624	-1.89881	470.95	903.01
9	-5.13588	-3.64252	-1.49336	512.36	1224.44
10	-5.01207	-2.88223	-2.12984	436.21	701.13

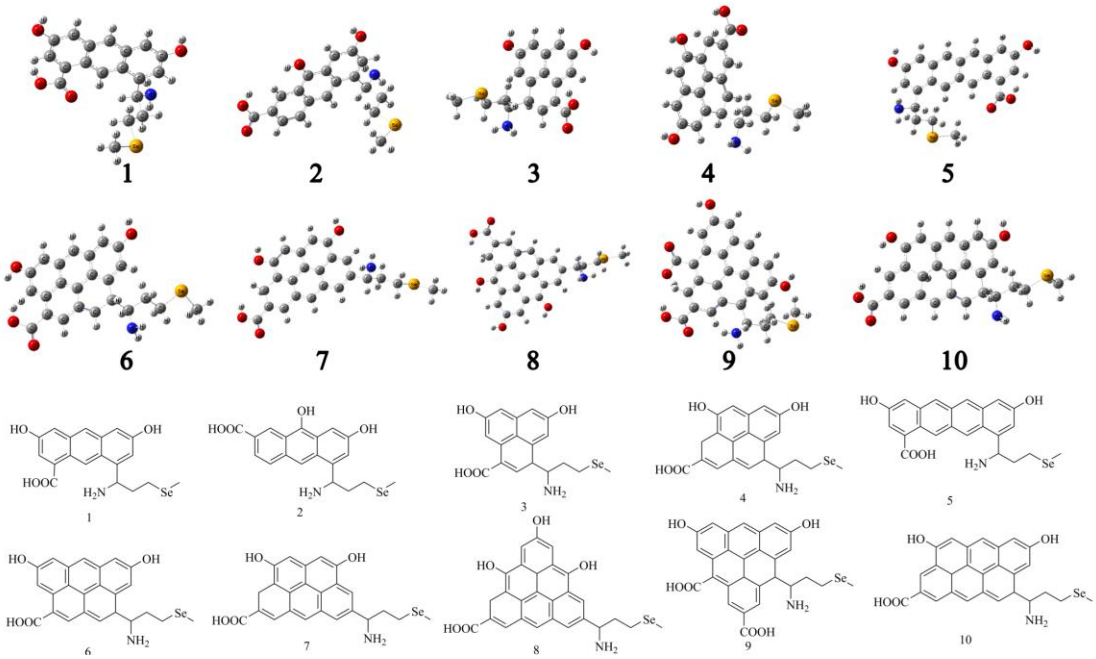

Fig. S29. The optimized structures of the possible structures of the CDs.

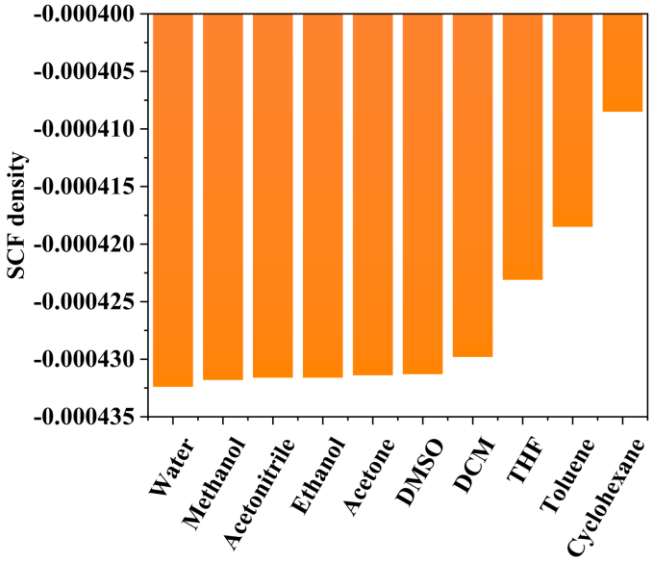

Fig. S30. SCF density of the optimized structure of the CDs in different polarity of solvents.

Table S4. The calculated HOMO and LUMO energy of the CDs at S0 state in solvents with different polarity.

S0	Polarity	HOMO (eV)	LUMO (eV)	△ (eV)
Water	0.321	-5.66841	-2.24140	-3.42700
Methanol	0.309	-5.71004	-2.26154	-3.44850
Acetonitrile	0.305	-5.76446	-2.26453	-3.49993
Ethanol	0.290	-5.76929	-2.23460	-3.53469
Acetone	0.284	-5.83581	-2.24031	-3.59550
Dimethylsulfoxide	0.264	-5.87004	-2.23759	-3.63245
Dichloromethane	0.217	-5.91902	-2.23814	-3.68089
Tetrahydrofuran	0.209	-5.95576	-2.23977	-3.71599
Cyclohexane	-0.002	-5.96664	-2.24031	-3.72633

Table S5. The calculated HOMO and LUMO energy of the CDs at S1 state in solvents with different polarity.

S1	Polarity	HOMO (eV)	LUMO (eV)	△ (eV)
Water	0.321	-5.01207	-2.88223	-2.12984
Methanol	0.309	-5.06676	-2.88142	-2.18535
Acetonitrile	0.305	-5.06676	-2.87924	-2.18752
Ethanol	0.290	-5.06676	-2.87706	-2.18970
Acetone	0.284	-5.06676	-2.87570	-2.19106
Dimethylsulfoxide	0.264	-5.06649	-2.86971	-2.19678
Dichloromethane	0.217	-5.06785	-2.86672	-2.20113
Tetrahydrofuran	0.209	-5.06867	-2.86427	-2.20440
Cyclohexane	-0.002	-5.08799	-2.84822	-2.23977

Table S6. The calculated HOMO and LUMO energy gaps of the CDs in solvents with different polarity.

S1	Polarity	HOMO of S0 (eV)	LUMO of S1 (eV)	△ (eV)
Water	0.321	-5.66841	-2.88223	-2.78618
Methanol	0.309	-5.71004	-2.88142	-2.82863
Acetonitrile	0.305	-5.76446	-2.87924	-2.88522
Ethanol	0.290	-5.76929	-2.87706	-2.89223
Acetone	0.284	-5.83581	-2.87570	-2.96011
Dimethylsulfoxide	0.264	-5.87004	-2.86971	-3.00033
Dichloromethane	0.217	-5.91902	-2.86672	-3.05230
Tetrahydrofuran	0.209	-5.95576	-2.86427	-3.09149
Cyclohexane	-0.002	-5.96664	-2.84822	-3.11843

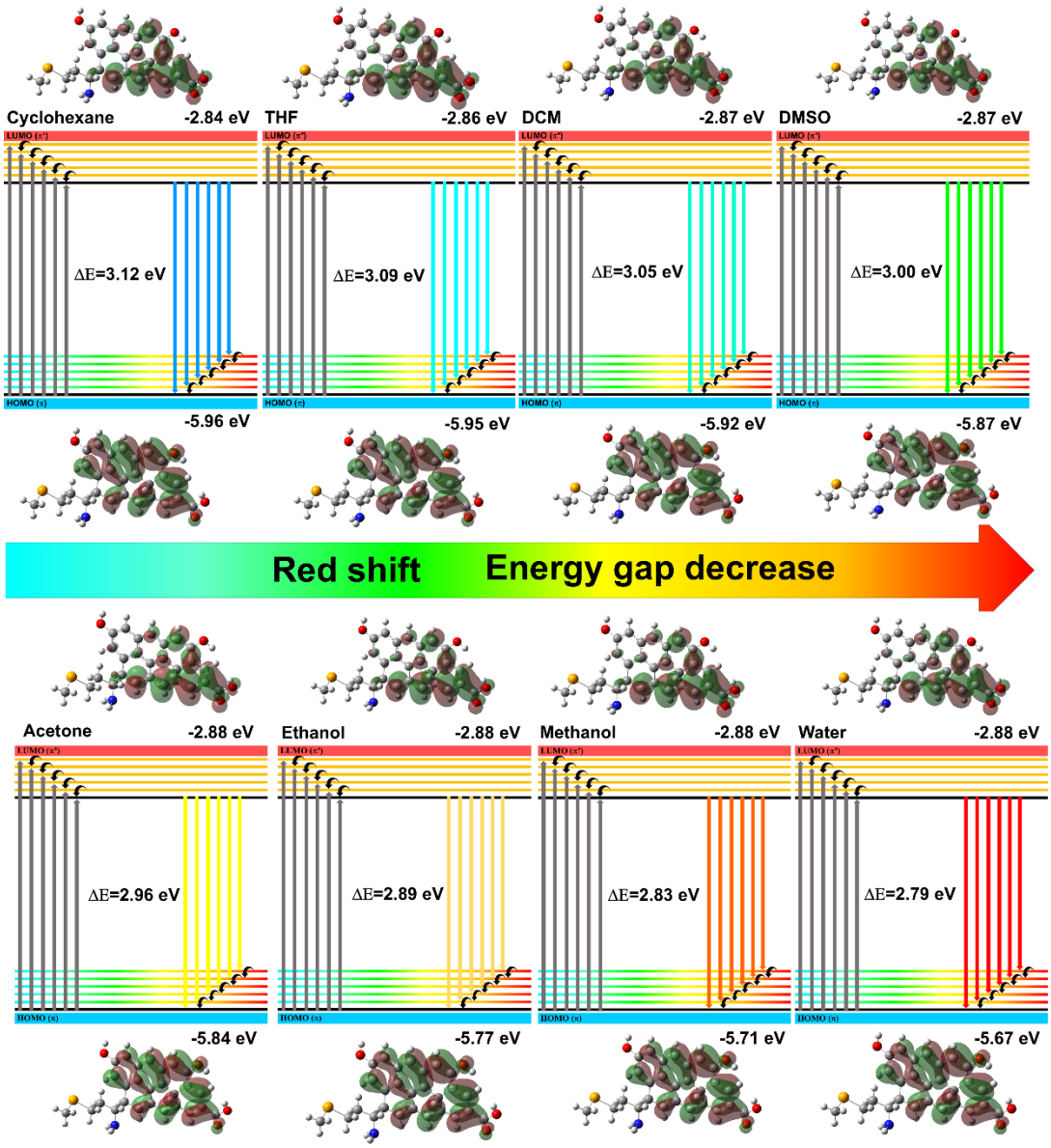

Fig. S31. HOMO and LUMO energies and orbitals of the optimized structure of the CDs in solvents of different polarities.

5. Polarity imaging in living cells.

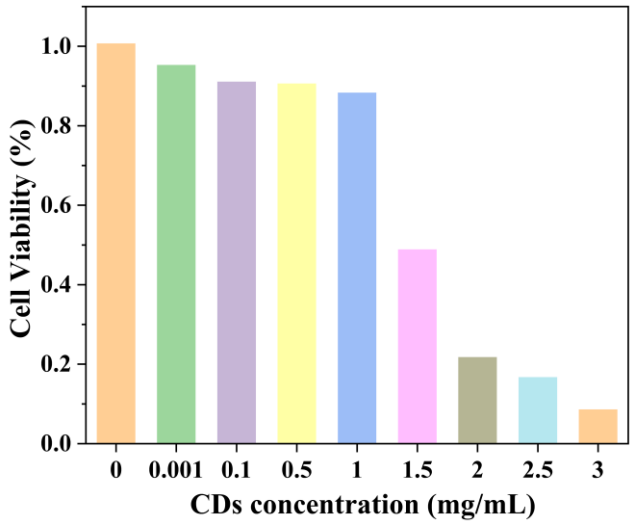

Fig. S32. IC50 detection of cell viability with the change of the CDs concentration.

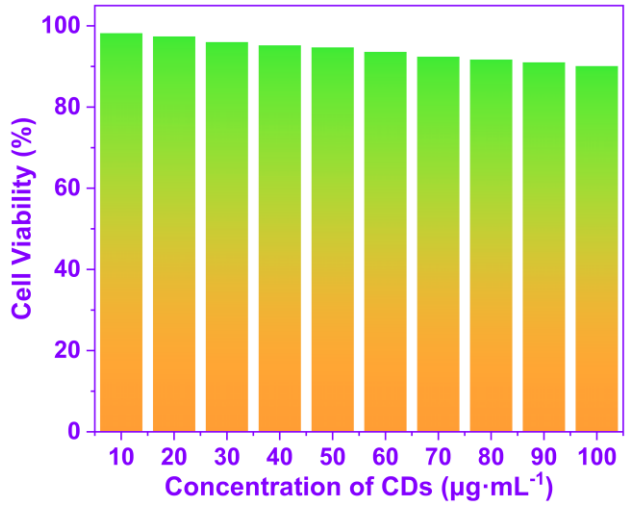

Fig. S33. The influence of cell viability with the change of the CDs concentration.

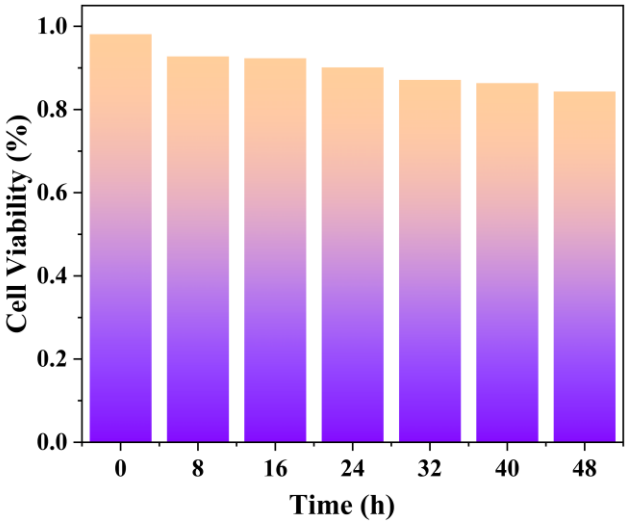

Fig. S34. The influence of cell viability with the change of time.

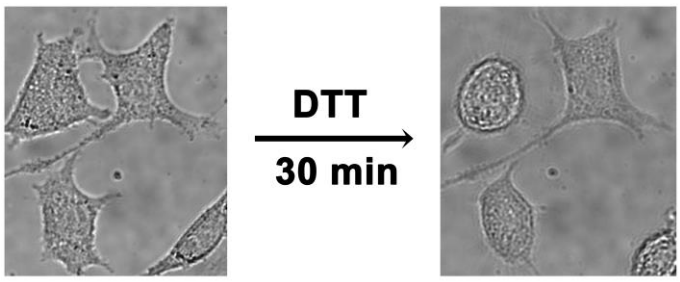

Fig. S35. Bright-field images of HeLa, cells after treatment with 5 mmol L^{-1} DTT for 30 min.

6. ^{1}H NMR spectrum of the CDs.

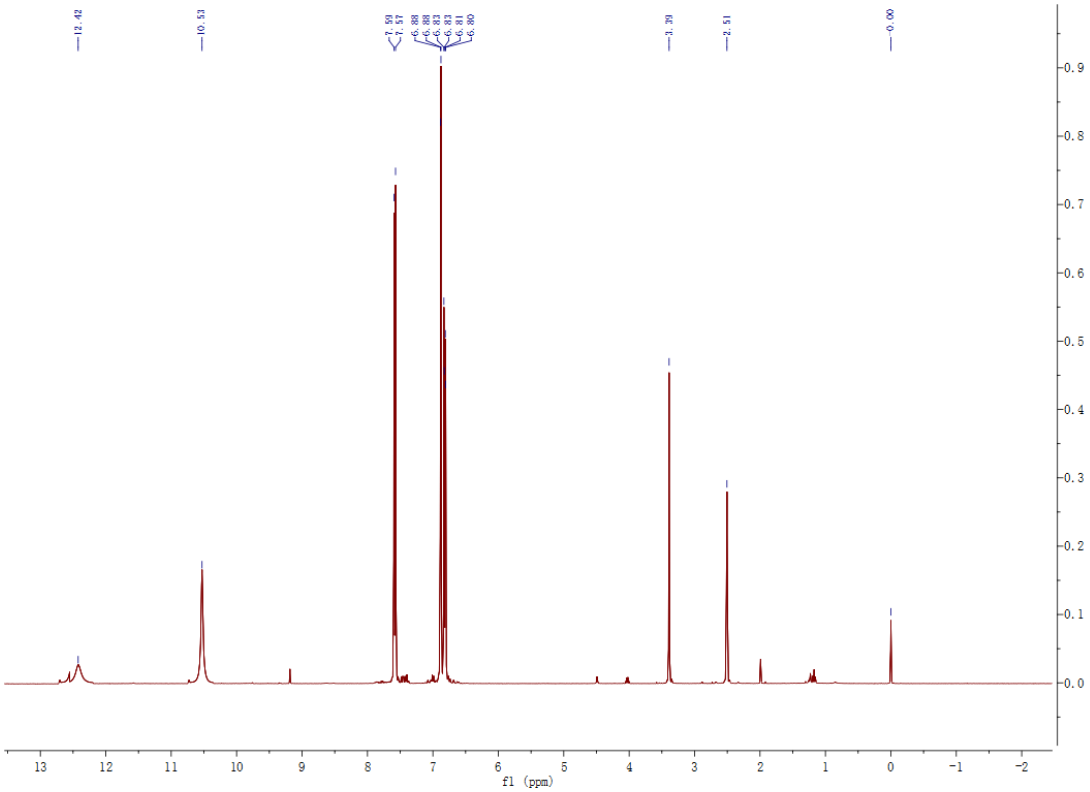

Fig. S36. ^{1}H NMR spectrum of the CDs in DMSO-d6.

7. Comparison of the CDs with other reported methods

Table S7. Comparison of the N, Se-CDs for the detection of polarity and LDs with other reported CDs probes

CDs	LOD		Emission wavelength	Quantum yield	Response time	Response target	Pearson coefficient	Reference
PS-CDs	0.03	0.03-0.229	600 nm	21%	-	polarity LDs cytoplasm	- 0.90 0.60	[1]
R-CDs	0.013	0.013-0.321	612 nm	47.87%	-	polarity Lysosomes Mitochondria	- 0.88 0.72	[2]
R-CDs		-	640 nm	37.2%	-	polarity	-	[3]
r-bCDs	0.02	0.020-0.315	588 nm	-	-	polarity Lysosomal	- 0.89, 0.92, 0.93	[4]
Phenyl-CDs	0.23	0.230−0.300	595 nm	10.5%	-	polarity Lysosome	0.93	[5]
PPh-CDs	0.23	-	620 nm	1.77%	-	polarity Lysosome	0.87	[6]
Ni−pPCDs	-	-	605 nm	64.9%	-	polarity RNA、DNA	-	[7]
PCDs	0.189	0.189-0.229	572 nm	-	-	polarity	-	[8]
CDs-3	0.021	0.021-0.32	470 nm	0.87	-	ER polarity	0.85	[9]
CPDs	-	-	631 nm	84.23%	3 min	polarity LDs	0.903	[10]
o-CDs	-	-	601 nm	1.75%	-	polarity	-	[11]
N, Cl-CDs	0.093	0.209-0.320	568 nm	21.8%	-	polarity	-	[12]
N, S-CDs	0.209	0.262-0.321	640 nm	27.65%	10 s	polarity Lysosomes Mitochondria	- 0.65 0.75	[13] JMCA
N, Se-CDs	**0.021**	**0.201-0.321**	**700 nm**	**32.45%**	**1 s**	**polarity LDs Lysosomes Mitochondria**	**0.96 0.89 0.85**	**This work**

Table S8. Comparison of the N, Se-CDs for the detection of polarity and LDs with other reported organic probes

Probes	LOD	Linear range	Emission wavelength	Quantum yield	Response target	Pearson coefficient	Reference
NOH	0.124	0.124-0.316	474 nm 552 nm	-	Lysosome polarity	0.97	[14]
1a 1b	ET(30) =33.9	ET(30)=33.9-55.4	541 nm (MeOH) 570 nm (MeOH)	0.73 (DMSO) 0.87 (DMSO)	LDs polarity	0.94 0.90	[15]
PI-CHO	ET(30) = 37.4	ET(30)= 37.4-63.1	580 nm	74.13% (THF)	LDs polarity	0.85	[16]
HPB derivatives	-	-	596 nm (CH_2Cl_2) 593 nm (CH_3CN)	0.86 (CH_2Cl_2) 0.77 (C_6H_{12}) 0.91 (C7H8）	polarity	-	[17]
ATOP-LD	-	-	493 nm (DMSO)	0.76 (CH_2Cl_2) 21.9% (toluene)	LDs polarity	0.95	[18]
CX-P	0.284	0.284-0.321	>650 nm	-	polarity	-	[19]
DCM-ML	0.229	0.229-0.31	705 nm	-	Lysosomal polarity	0.902	[20]
LW-1	-	-	642 nm(CH_3CN)	-	LDs polarity	0.976	[21]
CCB	ET(30) =33.9	ET(30)=33.9-45.6	659 nm	-	LDs polarity	0.89	[22]
LD-HW	0.32	0.3200-0.0205	689 nm	70.62% (1,4-dioxane) 0.16% (water)	LDs polarity	0.91、0.90	[23]
NIR-BT-P	0.25	0.250-0.298	853 nm	-	Mitophagy polarity	0.85	[24]
PNN	ET(30) =33.9	ET(30)=33.9-45.1	582.5 nm	34% (toluene)	Mitophagy polarity	0.95	[25]
LDs-CA LDs-BCA	1%	1%-90%	636 nm 678 nm	-	LDs polarity	0.9614 0.8394	[26]
LD-TTP	0.258	0.258-0.312	548 nm	-	LDs polarity	0.91	[27]
Hcy-Rh	7.13	7.13−8.44	450 nm 580 nm	31.77%-8.08% (pH2.52-10.50)	pH LDs Mitophagy Lysosome polarity	0.92 0.95 0.58	[28]
TICT-lipid	ET(30) =33.9	ET(30)=33.9-45.6	634 nm	-	polarity	-	[29]
Mem-C_1C_{18} Mem-$C_{18}C_{18}$	0.210	0.210-0.333	626 nm 614 nm	0.757 (CH_2Cl_2) 0.616 (DMSO)	polarity	-	[30]

lip-YB	-	-	650 nm	73.28%	LDs polarity	0.91	[31]
LDs-Red	ET(30) =33.9	ET(30)=33. 9-45.6	717 nm	83% (toluene)	LDs polarity	0.95	[32]
LCP	-	-	500 nm 662 nm	-	Lysosome polarity	0.91	[33]
COP	0.186	0.186-0.321	679 nm	-	polarity	0.85	[34]
ER-NAPC	130 nM	0 - 10 μM	545 nm	0.39	$O^{2\cdot-}$ polarity	0.92	[35]
DAF	ET(30) =33.9	ET(30)=33. 9-55.4	550 nm	0.97	LDs polarity	0.6995 ± 0.0154	[36]
Golgi-P	-	-	810 nm	-	Golgi apparatus polarity	0.93	[37]
DPDO-C	-	-	800 nm	37.82%	Mitophagy LDs polarity	0.92 0.91	[38]
BNT NPs BseNT NPs	-	-	930 nm 985 nm	49.2% 17.3%	LDs polarity	0.92	[39]
Probe 1	0.027	0.027-0.290	704 nm	-	LDs polarity	0.90	[40]
CQPP	-	-	671 nm	-	ROS LDs polarity	0.92	[41]
BOB	0.013	0.013-0.32	467 nm 642 nm	-	Mitophagy polarity	0.96	[42]
MLD-1	-	-	560 nm	0.85	Mitophagy LDs polarity	0.95 0.90	[43]
CTPA	ET(30) =33.9	ET(30)=33. 9-45.1	620 nm	20.1%	LDs polarity	0.94	[44]
CPM	0.209	0.209-0.209	620 nm	-	Lysosome polarity	0.93	[45]
MND-Lys	ET(30) =33.9	ET(30)=33. 9-45.1	-	30.8% (toluene)	Lysosome polarity	96.3%	[46]
HXPI - P	ε=4.36	ε=4.36-80.1	724 nm	-	Mitophagy polarity	0.97	[47]
ZIF-90@Si R	0.34 mM	1 - 7 mM	670 nm	-	ATP	-	[48]
DC-Lyso	-	-	640 nm	0.10 ±0.3%	Lysosome polarity	0.93	[49]
ICM	-	-	480 nm 690 nm	0.79	Mitophagy LDs polarity	0.89 0.87	[50]
P1	0.021	0.021-0.209	700 nm	0.68	LDs polarity	0.97	[51]
PPTH	0.17	0.17-0.25	633 nm	1.62%	LDs polarity	0.94、0.92	[52]

DEA-Fl-CN	0.0206	0.0206-0.209	-	-	Polarity the TPM content	-	[53]
LIP-Ser	ET(30)=33.9	ET(30)=33.9-45.6	634 nm-	0.415	ROS LDs polarity	0.97	[54]
MQA-DNP	0.0205	0.0205-0.3200	634 nm 714-786 nm	4.904%	H_2S polarity	0.92	[55]
DCIMe DCIJ DCIQ	-	-	604 – 687 nm 630 – 725 nm 679 – 811 nm	-	LDs polarity	0.95 0.93 0.94	[56]
AP-NAP AP-NR	-	-	619 ~ 729 nm 604 ~ 647 nm	-	Lysosome polarity	0.94 0.90	[57]
TP-LDs	0.136	0.136-0.273	508 ~ 618 nm	-	LDs polarity	0.93	[58]
ZP-1	0.0205	0.0205-0.3200	406 ~ 566 nm	70.9 ~ 1.9% (Diox-H_2O)	LDs polarity	0.92、0.90	[59]
TPA-DCPP（NPS）	0.363	0.363-0.381	470 ~ 850 nm	--	Lysosome polarity	0.94	[60]
TBPCPP	0.015	0.015-0.265	580 ~ 667 nm	0.89 ~ 0.15 (Tol-DMSO)	LDs polarity	0.98	[61]
LD-B	0.0245	0.0245-0.311	635 -679 nm 642-680nm	-	LDs polarity	0.8586	[62]
SNL	0.022	0.022-0.288	758 ~ 812 nm	-	Lysosome polarity	0.91	[63]
N, Se-CDs	**0.021**	**0.201-0.321**	**700 nm**	**32.45%**	**polarity LDs Lysosomes Mitochondria**	**0.96 0.89 0.85**	**This work**

8. References

[1] J. Hu, Y. Sun, X. Geng, J. Wang, Y. Guo, L. Qu, K. Zhang, Z. Li, High-fidelity carbon dots polarity probes: revealing the heterogeneity of lipids in oncology, Light: Sci. Appl. 11(1) (2022) 185.

[2] X. Shi, Y. Hu, H.-M. Meng, J. Yang, L. Qu, X.-B. Zhang, Z. Li, Red emissive carbon dots with dual targetability for imaging polarity in living cells, Sensor. Actuat. B-Chem. 306 (2020) 127582.

[3] W. Zhou, C. Liu, J. Fan, J. Luo, L. Liu, J. Huang, R. Liu, X. Zhang, Red-emitting carbon dots as luminescent agent in wide-range water detection in organic solvents and polarity-selective zebrafish imaging, J. Alloys Compd. 920 (2022) 165963.

[4] G. Zou, S. Chen, N. Liu, Y. Yu, A ratiometric fluorescent probe based on carbon dots assembly for intracellular lysosomal polarity imaging with wide range response, Chin. Chem. Lett. 33(2) (2022) 778-782.

[5] Y. Sun, H. Qin, X. Geng, R. Yang, L. Qu, A.N. Kani, Z. Li, Rational Design of Far-Red to Near-Infrared Emitting Carbon Dots for Ultrafast Lysosomal Polarity Imaging, ACS Appl. Mater. Interfaces 12(28) (2020) 31738-31744.

[6] J. Hu, R. Yang, H. Qin, Y. Sun, L. Qu, Z. Li, Spying on the Polarity Dynamics during Wound Healing of Zebrafish by Using Rationally Designed Carbon Dots, Adv. Healthc. Mater. 10(14) (2021) 2002268.

[7] X.-W. Hua, Y.-W. Bao, J. Zeng, F.-G. Wu, Nucleolus-Targeted Red Emissive Carbon Dots with Polarity-Sensitive and Excitation-Independent Fluorescence

Emission: High-Resolution Cell Imaging and in Vivo Tracking, ACS Appl. Mater. Interfaces 11(36) (2019) 32647-32658.

[8] J.H. Liu, D.Y. Li, J.H. He, D. Yuan, R.S. Li, S.J. Zhen, Y.F. Li, C.Z. Huang, Polarity-Sensitive Polymer Carbon Dots Prepared at Room-Temperature for Monitoring the Cell Polarity Dynamics during Autophagy, ACS Appl. Mater. Interfaces 12(4) (2020) 4815-4820.

[9] E. Shuang, Q.-X. Mao, J.-H. Wang, X.-W. Chen, Carbon dots with tunable dual emissions: from the mechanism to the specific imaging of endoplasmic reticulum polarity, Nanoscale 12(12) (2020) 6852-6860.

[10] Z. Huo, X. Cao, D. Sun, W. Xu, B. Yang, S. Xu, Carbonized Polymer Dot Probe for Two-Photon Fluorescence Imaging of Lipid Droplets in Living Cells and Tissues, ACS Sens. 8(5) (2023) 1939-1949.

[11] Y. Meng, S. Cui, P. Lei, J. Guo, Q. Wang, S. Shuang, C. Dong, Design of polarity-dependence orange emission multifunctional carbon dots for water detection and anti-counterfeiting, Mater. Today Chem. 33 (2023) 101669.

[12] J. Jia, W. Lu, S. Cui, C. Dong, S. Shuang, N, Cl-doped carbon dots for fluorescence and colorimetric dual-mode detection of water in tetrahydrofuran and development of a paper-based sensor, Microchim. Acta 188(10) (2021) 324.

[13] Z. Yang, H. Li, T. Xu, M. She, J. Chen, X. Jia, P. Liu, X. Liu, J. Li, Red emissive carbon dots as a fluorescent sensor for fast specific monitoring and imaging of polarity in living cells, J. Mater. Chem. A 11(6) (2023) 2679-2689.

[14] M. Li, J. Fan, H. Li, J. Du, S. Long, X. Peng, A ratiometric fluorescence probe

for lysosomal polarity, Biomaterials 164 (2018) 98-105.

[15] C. Yu, X. Guo, X. Fang, N. Chen, Q. Wu, E. Hao, L. Jiao, Efficiently emissive, strongly solvatochromic and lipid droplet-specific, fluorescent probes for mapping polarity *in vitro*, Dyes Pigm. 197 (2022) 109838.

[16] X. Ma, H. Yu, M. Wang, M. Li, X. Feng, M. Shao, Q. Zhang, F. Zhong, An imidazole-derived polarity sensitive probe for lipid droplet target and in vivo tumor imaging, Talanta 252 (2023) 123903.

[17] G. Yin, Y. Li, S. Li, B. Xu, Q. Yang, Y. Zhang, J. Zhao, X. Cao, Hexaphenylbenzene based push-pull fluorophores displaying intriguing polarity-dependent fluorescence behavior, AIE (E) characteristics and mega-large Stokes shifts, Dyes Pigm. 198 (2022) 110013.

[18] W.-L. Cui, M.-H. Wang, X.-Q. Chen, Z.-H. Zhang, J. Qu, J.-Y. Wang, A novel polarity-sensitive fluorescent probe for lighting up lipid droplets and its application in discriminating dead and living zebrafish, Dyes Pigm. 204 (2022) 110433.

[19] W.-X. Wang, Z.-Q. Wang, Z.-K. Tan, K.-Y. Guo, G.-J. Mao, Y. Li, C.-Y. Li, A tumor-targeting and polarity-specific near-infrared fluorescent probe for accurate cancer diagnosis in vivo, Dyes Pigm. 206 (2022) 110612.

[20] X. Chao, Y. Hu, R. Liu, D. Huang, Y. Zhang, Near-infrared ratiometric fluorescence imaging of lysosomal polarity in live cells and *in vivo*, Sensor. Actuat. B-Chem. 345 (2021) 130397.

[21] C. Liu, J. Yin, B. Lu, W. Lin, Tracking the polarity changes of asthmatic mice by

fluorescence imaging, Sensor. Actuat. B-Chem. 346 (2021) 130448.

[22] C. Lai, Y. Zhao, X. Zou, Y. Liang, W. Lin, Quantification of lipid droplets polarity for evaluating non-alcoholic fatty liver disease via fluorescence lifetime imaging, Sensor. Actuat. B-Chem. 369 (2022) 132267.

[23] L. Hu, J. Pan, C. Zhang, K. Yu, S. Shen, Y. Wang, X. Shen, X. Gu, J. Han, H. Wang, Polarity-sensitive and lipid droplet-specific red emission fluorophore for identifying fatty liver of living mice through *in vivo* imaging, Biosens. Bioelectron. 216 (2022) 114618.

[24] T. Zhang, F. Huo, W. Zhang, F. Cheng, C. Yin, Development of near-infrared mitochondrial polarity fluorescent probe for evaluating mitophagy in mice heart and potential cancer diagnosis, Chem. Eng. J. 437 (2022) 135397.

[25] J. Yin, X. Lin, Q. Hu, S. Huang, Mitochondrial polarity-triggered fluorogenic optical agent for exploring breast cancer, Chem. Eng. J. 450 (2022) 138282.

[26] C. Lai, Y. Zhao, Y. Liang, X. Zou, W. Lin, BF_2 group chelated AIE fluorescent probe for polarity mapping of lipid droplets in cells and in *vivo*, Spectrochim. Acta A 268 (2022) 120637.

[27] L. Fan, X. Wang, Q. Zan, L. Fan, F. Li, Y. Yang, C. Zhang, S. Shuang, C. Dong, Lipid Droplet-Specific Fluorescent Probe for *In Vivo* Visualization of Polarity in Fatty Liver, Inflammation, and Cancer Models, Anal. Chem. 93(22) (2021) 8019-8026.

[28] Q. Bai, C. Yang, M. Yang, Z. Pei, X. Zhou, J. Liu, H. Ji, G. Li, M. Wu, Y. Qin, Q. Wang, L. Wu, pH-Dominated Selective Imaging of Lipid Droplets and

Mitochondria via a Polarity-Reversible Ratiometric Fluorescent Probe, Anal. Chem. 94(6) (2022) 2901-2911.

[29] C. Wang, J. Wang, K. Xue, M. Xiao, K. Wu, S. Lv, B. Hao, C. Zhu, Polarity-Sensitive Fluorescent Probe for Reflecting the Packing Degree of Bacterial Membrane Lipids, Anal. Chem. 94(7) (2022) 3303-3312.

[30] S. Wu, Y. Yan, H. Hou, Z. Huang, D. Li, X. Zhang, Y. Xiao, Polarity-Sensitive and Membrane-Specific Probe Quantitatively Monitoring Ferroptosis through Fluorescence Lifetime Imaging, Anal. Chem. 94(32) (2022) 11238-11247.

[31] H. Huang, Y. Bu, Z.-P. Yu, M. Rong, R. Li, Z. Wang, J. Zhang, X. Zhu, L. Wang, H. Zhou, Solvatochromic Two-Photon Fluorescent Probe Enables *In Situ* Lipid Droplet Multidynamics Tracking for Nonalcoholic Fatty Liver and Inflammation Diagnoses, Anal. Chem. 94(39) (2022) 13396-13403.

[32] G. Peng, J. Dai, R. Zhou, G. Liu, X. Liu, X. Yan, F. Liu, P. Sun, C. Wang, G. Lu, Highly Efficient Red/NIR-Emissive Fluorescent Probe with Polarity-Sensitive Character for Visualizing Cellular Lipid Droplets and Determining Their Polarity, Anal. Chem. 94(35) (2022) 12095-12102.

[33] L. Huang, L. Zhu, W. Su, X. Liang, W. Li, W. Lin, Novel Polarity Fluorescent Probe for Dual-Color Visualization of Lysosomes and Plasma Membrane during Apoptosis, Anal. Chem. 94(33) (2022) 11643-11649.

[34] Q. Li, J. Hong, S. Feng, S. Gong, G. Feng, Polarity-Sensitive Cell Membrane Probe Reveals Lower Polarity of Tumor Cell Membrane and Its Application for Tumor Diagnosis, Anal. Chem. 94(31) (2022) 11089-11095.

[35] H. Xiao, C. Wu, P. Li, B. Tang, Simultaneous Fluorescence Visualization of Endoplasmic Reticulum Superoxide Anion and Polarity in Myocardial Cells and Tissue, Anal. Chem. 90(10) (2018) 6081-6088.

[36] M. Collot, S. Bou, T.K. Fam, L. Richert, Y. Mély, L. Danglot, A.S. Klymchenko, Probing Polarity and Heterogeneity of Lipid Droplets in Live Cells Using a Push–Pull Fluorophore, Anal. Chem. 91(3) (2019) 1928-1935.

[37] P. Li, X. Guo, X. Bai, X. Wang, Q. Ding, W. Zhang, W. Zhang, B. Tang, Golgi Apparatus Polarity Indicates Depression-Like Behaviors of Mice Using in Vivo Fluorescence Imaging, Anal. Chem. 91(5) (2019) 3382-3388.

[38] S. Wang, M. Zhou, L. Chen, M. Ren, Y. Bu, J. Wang, Z.-P. Yu, X. Zhu, J. Zhang, L. Wang, H. Zhou, Polarity-Sensitive Probe: Dual-Channel Visualization of the "Chameleon" Migration with the Assistance of Reactive Oxygen Species, ACS Appl. Bio Mater. 5(7) (2022) 3554-3562.

[39] X. Zhou, K. Zhang, C. Yang, Y. Pei, L. Zhao, X. Kang, Z. Li, F. Li, Y. Qin, L. Wu, Ultrabright and Highly Polarity-Sensitive NIR-I/NIR-II Fluorophores for the Tracking of Lipid Droplets and Staging of Fatty Liver Disease, Adv. Funct. Mater. 32(12) (2022) 2109929.

[40] D. He, M. Yan, Q. Sun, M. Zhang, Y. Xia, Y. Sun, Z. Li, Ketocyanine-Based Fluorescent Probe Revealing the Polarity Heterogeneity of Lipid Droplets and Enabling Accurate Diagnosis of Hepatocellular Carcinoma, Adv. Healthc. Mater. 13(7) (2024) 2303212.

[41] K.-N. Wang, L.-Y. Liu, D. Mao, S. Xu, C.-P. Tan, Q. Cao, Z.-W. Mao, B. Liu, A

Polarity-Sensitive Ratiometric Fluorescence Probe for Monitoring Changes in Lipid Droplets and Nucleus during Ferroptosis, Angew. Chem. Int. Ed. 60(27) (2021) 15095-15100.

[42] N. Jiang, J. Fan, F. Xu, X. Peng, H. Mu, J. Wang, X. Xiong, Ratiometric Fluorescence Imaging of Cellular Polarity: Decrease in Mitochondrial Polarity in Cancer Cells, Angew. Chem. Int. Ed. 54(8) (2015) 2510-2514.

[43] S. Biswas, M. Baruah, A. Shil, S. Sarkar, M. Ali, A. Samanta, S. Bhuniya, Polarity-Driven Two-Photon Fluorescent Probe for Monitoring the Perturbation in Lipid Droplet Levels during Mitochondrial Dysfunction and Acute Pancreatitis, ACS Sens. 8(10) (2023) 3793-3803.

[44] J. Yin, M. Peng, Y. Ma, R. Guo, W. Lin, Rational design of a lipid-droplet-polarity based fluorescent probe for potential cancer diagnosis, Chem. Commun. 54(85) (2018) 12093-12096.

[45] L. Fan, X. Wang, J. Ge, F. Li, X. Wang, J. Wang, S. Shuang, C. Dong, A lysosome-targeting and polarity-specific fluorescent probe for cancer diagnosis, Chem. Commun. 55(32) (2019) 4703-4706.

[46] J. Yin, M. Peng, W. Lin, Tracking lysosomal polarity variation in inflamed, obese, and cancer mice guided by a fluorescence sensing strategy, Chem. Commun. 55(74) (2019) 11063-11066.

[47] X. Li, X. Li, H. Ma, A near-infrared fluorescent probe reveals decreased mitochondrial polarity during mitophagy, Chem. Sci. 11(6) (2020) 1617-1622.

[48] J.-T. Chen, S.-S. Chen, Z.-Q. Wang, G. Yu, G.-J. Mao, J. Fei, C.-Y. Li,

Near-Infrared Fluorescent Nanoprobes for Adenosine Triphosphate-Guided Imaging in Cancer and Fatty Liver Mice, Anal. Chem. 95(3) (2023) 2119-2127.

[49] S. Das, A. Batra, S. Kundu, R. Sharma, A. Patra, Unveiling autophagy and aging through time-resolved imaging of lysosomal polarity with a delayed fluorescent emitter, Chem. Sci. 15(1) (2024) 102-112.

[50] J. Hong, J. Zhang, Q. Li, G. Feng, One stone, three birds: a smart single fluorescent probe for simultaneous and discriminative imaging of lysosomes, lipid droplets, and mitochondria, Anal. Chem. 95(5) (2023) 2671-2679.

[51] J.-T. Hou, C. Li, S. Guo, X. Ye, W. Chi, Y. Ren, Q. Wang, J. Shen, Polarity-Driven Fluorescence Monitoring of Lipid Droplet Dynamics in Dry Eye Disease, Anal. Chem. 96(24) (2024) 9975-9983.

[52] X. Tian, D. Wu, W. Wei, G. Dai, Z. Li, B. Wang, M. Yu, A lipid droplets-targetable fluorescent probe for polarity detection in cells of iron death, inflammation and fatty liver tissue, Chin. Chem. Lett. 35(6) (2024) 108912.

[53] Y. Kang, Y. Sun, L. Qu, Z. Li, Engineering of polarity-responsive fluorescent probe for real-time measurement and visualization of total polar materials in edible oils, Sensor. Actuat. B-Chem. 392 (2023) 134100.

[54] W. Wang, L. Chai, X. Chen, Z. Li, L. Feng, W. Hu, H. Li, G. Yang, Imaging changes in the polarity of lipid droplets during NAFLD-Induced ferroptosis via a red-emitting fluorescent probe with a large Stokes shift, Biosens. Bioelectron. 231 (2023) 115289.

[55] Q. Zan, L. Fan, L. Ma, Q. Yang, K. Zhao, Y. Huang, C. Dong, S. Shuang,

Dual-channel fluorescent probe for simultaneously detecting H_2S and viscosity/polarity and its application in non-alcoholic fatty liver, tumor tissue, and food spoilage, Sensor. Actuat. B-Chem. 397 (2023) 134596.

[56] J. Hong, Y. Liu, X. Tan, G. Feng, Engineering of a NIR fluorescent probe for high-fidelity tracking of lipid droplets in living cells and nonalcoholic fatty liver tissues, Biosens. Bioelectron. 240 (2023) 115646.

[57] H. Xue, W. Ge, T. Li, M. Yan, M. Tian, Polarity-responsive probe distinguishing different apoptotic stages in three distinct sets of fluorescence signals, Sensor. Actuat. B-Chem. 398 (2024) 134714.

[58] Y. Pu, R. Huang, L. Chai, H. Yang, D. Wang, Z. Wei, Z. Zhan, Multimode evaluating the fluctuation of lipid droplets polarity in acute kidney injury and tumor models, Sensor. Actuat. B-Chem. 380 (2023) 133343.

[59] T. Liu, J. Chen, Y. Dai, Z. Wang, P. Chen, Y. Zhou, H. Wang, Y. Li, Z. Mo, C. Yang, X. Zhang, B. Sun, J. Yin, L. Li, G. Li, J. Ma, Harnessing polarity-dependent fluorescent probe for lipid droplet metabolism dissection and in vivo nonalcoholic fatty liver disease diagnosis, Sensor. Actuat. B-Chem. 399 (2024) 134825.

[60] T. Wu, L. Duan, J. Yang, Y. Zhou, A multidimensional quantitative fluorescent probe for high-fidelity monitoring of the polarity change in lysosomes during autophagy, Sensor. Actuat. B-Chem. 393 (2023) 134142.

[61] J. Sha, W. Liu, X. Zheng, Y. Guo, X. Li, H. Ren, Y. Qin, J. Wu, W. Zhang, C.-S. Lee, P. Wang, Polarity-Sensitive Probe for Two-Photon Fluorescence Lifetime

Imaging of Lipid Droplets *In Vitro* and *In Vivo*, Anal. Chem. 95(41) (2023) 15350-15356.

[62] J. Zhang, W. Han, X. Zhou, X. Zhang, H. Zhang, T. Li, J. Wang, Y. Yuan, Y. He, J. Zhou, A Lipid Droplet-Specific NIR Fluorescent Probe with a Large Stokes Shift for In Vivo Visualization of Polarity in Contrast-Induced Acute Kidney Injury, Anal. Chem. 95(31) (2023) 11785-11792.

[63] J. Zhang, S. Gong, Q. Li, S. Zhang, G. Feng, Lysosome-Targeted Polarity-Sensitive NIR Fluorescence Probe for Imaging Injured Lung and Liver in Diabetes, Anal. Chem. 96(34) (2024) 14053-14059.